

This discussion paper is/has been under review for the journal Natural Hazards and Earth System Sciences (NHESD). Please refer to the corresponding final paper in NHESD if available.

# Dynamic variability examination of Mediterranean frontogenesis: teleconnection of fronts and flood 2010

B. A. Munir<sup>1</sup>, H. A. Imran<sup>2</sup>, and I. Ashraf<sup>3</sup>

<sup>1</sup>National Weather Forecasting Unit, Aviation Division, Pakistan Meteorological Department, Islamabad, Pakistan

<sup>2</sup>Environmental Protection and Agriculture Food Production, University of Hohenheim, Stuttgart, Germany

<sup>3</sup>Institute of GIS, School of Civil and Environmental Engineering, National University of Sciences and Technology, Islamabad, Pakistan

Received: 18 October 2015 – Accepted: 5 December 2015 – Published: 15 January 2016

Correspondence to: B. A. Munir (bilalahmedmunir35@gmail.com)

Published by Copernicus Publications on behalf of the European Geosciences Union.

## Dynamic variability examination of Mediterranean frontogenesis

B. A. Munir et al.

[Title Page](#)

[Abstract](#)

[Introduction](#)

[Conclusions](#)

[References](#)

[Tables](#)

[Figures](#)

[⏪](#)

[⏩](#)

[◀](#)

[▶](#)

[Back](#)

[Close](#)

[Full Screen / Esc](#)

[Printer-friendly Version](#)

[Interactive Discussion](#)









on the mid-latitudes of the Northern Hemisphere, latitudinal range is (30–65)° N and longitudinal range is (10–100)° E. The limits of the study area were selected as to minimize the distortion of spherical shape of satellites imagery. The study area includes Eurasia including countries; Cyprus, Egypt, Lebanon, Jordan, Syria, Turkey, Israel, Saudi Arabia, Iraq, Armenia, Georgia, Russia, Azerbaijan, Kazakhstan, Turkmenistan, Uzbekistan, Iran, Afghanistan and Pakistan.

Meteosat-7 satellite series secondary product was used for the identification of frontogenesis due to its free availability and for the coverage of full disc image in visible (0.55–1.05 μm), infra-red (10.2–12.5 μm) and water vapor (6.2–7.6 μm) band combination. VISSR (Visible and Infrared Spin Scan Radiometer) is a scanner carried aboard on the GMS (Geo-stationary Meteorological Satellite), stationed over Japan. The GMS imagery is re-broadcasted by Meteosat satellite. Whereas, precipitation data obtained from the derived product of TRMM (Tropical Rainfall Monitoring Mission) was used to analyze the resulting rainfall trends. The precipitation product was used to correlate the effects of frontogenesis in the major areas of interest. Main focus is on rain fall that is the major effect of frontal process.

## 2.1 Image classification

With the designed objectives full disc visualization of globe was needed for which geostationary satellite image is essential. Huge directory of individual band imagery (1.5 year) containing 1635 images were collected from December 2009 to August 2011 with temporal resolution of 1 day. The images were downloaded from the official website of the Dundee Satellite Station (Fig. 1). The images are of the sensor VISSR and the satellite has a slot of 57° E. The individual band was necessary as for the identification of pattern, moisture and thermal gradient present in the clouds.

The unsupervised classification was performed on each image of infra-red and water vapor bands. The identification process was based on the fundamentals of frontogenesis in 2-dimensional domains (sharp boundary of clouds in visible, thermal gradient in infra-red, and presence of moisture content in water vapor imagery) (Pike,

## Dynamic variability examination of Mediterranean frontogenesis

B. A. Munir et al.

[Title Page](#)

[Abstract](#)

[Introduction](#)

[Conclusions](#)

[References](#)

[Tables](#)

[Figures](#)

[⏪](#)

[⏩](#)

[◀](#)

[▶](#)

[Back](#)

[Close](#)

[Full Screen / Esc](#)

[Printer-friendly Version](#)

[Interactive Discussion](#)



1999); (Volkert, 1999); (Barry and Chorley, 2010); (Dirks et al., 1988); (Garabato et al., 2001); (Nieto et al., 2012).

Overlay scheme was used in ArcGIS environment for the identification of exact geographic locations where these fundamental parameters of frontogenesis meet in visible, infrared and water vapor bands. The overlay scheme was important as the assertion of frontogenesis should meet the three fundamentals.

## 2.2 Shift analysis

On average fronts have life cycles of 2–5 days. The foregoing research reports such frontal spells because these spells define the nature of frontogenesis well and good. Geographical location of the front was calculated on the starting and the ending day with the help of the two grids (default and manual grids). The shift was calculated as to analyze the geographical extent of the abundance of frontogenesis with the source of Mediterranean Sea fed by Atlantic Ocean. Basic formula of the range is used for the calculation of the latitudinal shifts

Geographical Shift = Difference between the position of first and the last day

To calculate the shift of the formation and trajectory of the fronts time series analysis done with certain time span. Finally, the movements of fronts are verified with the weather data included rain fall data for those area where these fronts hit in the areas of Pakistan and cause heavy rain fall in the year 2009, 2010 and 2011. The movement of frontal process was analyzed on daily basis with the calculation of velocity in  $^{\circ}\text{day}^{-1}$  by using the following equation:

$$\text{Velocity } (^{\circ}\text{day}^{-1}) = \frac{\text{Distance in } ^{\circ}}{\text{Time in days}}$$

## 2.3 Rainfall trends

To detect the rainfall patterns TRMM product was downloaded for the distinct spatial extent and range of the identified frontogenesis spells. The data was available for the

## Dynamic variability examination of Mediterranean frontogenesis

B. A. Munir et al.

[Title Page](#)

[Abstract](#)

[Introduction](#)

[Conclusions](#)

[References](#)

[Tables](#)

[Figures](#)

[⏪](#)

[⏩](#)

[◀](#)

[▶](#)

[Back](#)

[Close](#)

[Full Screen / Esc](#)

[Printer-friendly Version](#)

[Interactive Discussion](#)



latitudinal limits of 50° N to 50° S. The rainfall trends were analysed for the accumulated time period of 4 days because front has an average life span of 2–5 days. The rainfall patterns for the summer (July–August) and winter (December–January) season were examined to determine the areas and period of rainfall extremities. In keen rainfall trend for the same period was also observed throughout Pakistan on decadal basis to identify the contribution of these detected fronts in accentuating the rainfall pattern that caused flooding in Pakistan during July–August 2010.

### 3 Results and discussions

#### 3.1 Analysis of frontogenesis

Unsupervised classification algorithm with overlay scheme results in a directory of images that possesses the required fundamentals of fronts. The classified schemes shows five classes tiered on the basis of moisture content in the clouds and temperature of the clouds in water vapor and infra-red band respectively. It was observed that the abundance of clouds with moisture content and thermal gradient was mostly found in the tropical regions as these latitudes receive most perpendicular sun rays (Fig. 2) (Barry et al., 2009). The shift towards high latitudes was analyzed in summer due to the expansion of ITCZ. The ITCZ is a convergence field between the opposing trades that shows a seasonal variation just as do the trade winds.

It was scrutinized that different air masses scheme surrounds Eurasia throughout the year including maritime arctic (mA), maritime polar (mP), continental arctic (cA), continental polar (cP), maritime tropic (mT), and continental tropic (cT). The source regions, trajectories, and natural properties of individual air mass discerned the impacts associated with it. High abundance of moisture and thermal gradient was observed in cT during winter and summer with a source over North Africa (Aerographer, 2003).

## Dynamic variability examination of Mediterranean frontogenesis

B. A. Munir et al.

[Title Page](#)

[Abstract](#)

[Introduction](#)

[Conclusions](#)

[References](#)

[Tables](#)

[Figures](#)

[⏪](#)

[⏩](#)

[◀](#)

[▶](#)

[Back](#)

[Close](#)

[Full Screen / Esc](#)

[Printer-friendly Version](#)

[Interactive Discussion](#)





North Africa, Asia Minor, and South Balkans. This dynamic nature of air masses is cloned and observed for the frontogenesis in mid-latitudes.

In winter 2010 fronts formed in wide longitudinal range of almost  $33^\circ$  ( $33\text{--}66^\circ$ ) easts, while in 2011 this range decreases to  $12^\circ$  ( $55\text{--}67^\circ$ ) easts. However, in summers the two years (2010, 2011) show opposite behavior in winter. In 2011 record shift of  $49^\circ$  ( $20\text{--}69^\circ$ ) east was observed in the month of July, while in the summer of 2010 longitudinal shift is  $27^\circ$  ( $44\text{--}71^\circ$ ) east as shown in Fig. 3. The weather condition of a frontal system is well understood by analyzing the speed factor of frontal spell. Fast moving fronts usually cause more severe weather than slow moving fronts. Slow moving fronts, on the other hand, may cause extended periods of unfavorable weather (Aerographer, 2003; Barry et al., 1992). The results showed an inverse pattern of frontal speeds in winter and summer seasons for the respective years of 2010 and 2011. The average frontal speed of  $5.2^\circ \text{ day}^{-1}$ , and  $2.5^\circ \text{ day}^{-1}$  was observed in winter 2010 and 2011 respectively. However, increased average speed in winter by  $0.9^\circ \text{ day}^{-1}$  was observed in 2011 as compared to the year 2010 (Fig. 5).

Demonstrating the fundamental characteristics of frontal process, the recorded spells also shows pattern of retrograde motion in a spell of August 2010 in the vicinity of Pakistan. The motion was due to pressure disturbances in the path of the frontal scheme. The spell with a life span of 4 days shows  $65$ ,  $63$ ,  $66$ , and  $71^\circ \text{ E}$  longitudinal distributions.

### 3.3 Rainfall analysis

With  $0.25^\circ$  spatial and one day temporal resolution precipitation data from TRMM show best suitability to examine rainfall trends in the observed and defined geographical limits of frontogenesis for summer and winter seasons 2010. It was observed that during winter (December 2009–January 2010) rainfall maxima of 137 mm was experienced in Cyprus during 5–8 December which reached up to 207 mm from 9 to 12 December. Turkey and Iran were found observing up to 111 mm of rainfall from 17 to 20 December. While Cyprus, Lebanon, Syria and turkey were observed,

## Dynamic variability examination of Mediterranean frontogenesis

B. A. Munir et al.

[Title Page](#)

[Abstract](#)

[Introduction](#)

[Conclusions](#)

[References](#)

[Tables](#)

[Figures](#)



[Back](#)

[Close](#)

[Full Screen / Esc](#)

[Printer-friendly Version](#)

[Interactive Discussion](#)









## Dynamic variability examination of Mediterranean frontogenesis

B. A. Munir et al.

[Title Page](#)

[Abstract](#)

[Introduction](#)

[Conclusions](#)

[References](#)

[Tables](#)

[Figures](#)

[⏪](#)

[⏩](#)

[◀](#)

[▶](#)

[Back](#)

[Close](#)

[Full Screen / Esc](#)

[Printer-friendly Version](#)

[Interactive Discussion](#)



- Chelton, D. B., Schlax, M. G., Freilich, M. H., and Milliff, R. F.: Satellite measurements reveal persistent small-scale features in ocean winds, *Science*, 303, 978–983, 2004.
- Cione, J. J., Raman, S., and Pietrafesa, L. J.: The effect of Gulf Stream-induced baroclinicity on U.S. east coast winter cyclones, *Mon. Weather Rev.*, 121, 421–430, 1993.
- 5 Currie, K. I. and Hunter, K. A.: Surface water carbon dioxide in the waters associated with the subtropical convergence, east of New Zealand, *Deep-Sea Res. Pt. I*, 45, 1765–1777, 1998.
- Dirks, R. A., Kuettner, J. P., and Moore, J. A.: Genesis of Atlantic Lows Experiment (GALE): an overview, *B. Am. Meteorol. Soc.*, 69, 148–160, 1988.
- Frank, N. L.: On the energetics of cold lows, *Proceedings Symposium on Tropical Meteorology*, 2–11 June 1970, University of Huawei, Longgang District, Shenzhen city, China, *Amer. Meteor. SOC., EIV I–EIV 6*, 1970.
- 10 Garabato, A. C. N., Leach, H., Allen, J. T., Pollard, R. T., and Strass, V. H.: Mesoscale subduction at the Antarctic Polar Front driven by baroclinic instability, *J. Phys. Oceanogr.*, 31, 2087–2107, 2001.
- 15 Hopkins, J., Challenor, P., and Shaw, A. G. P.: A New Statistical Modelling Approach to Ocean Front Detection from SST Satellite Images, *Proudman Oceanographic Laboratory, Joseph Proudman, Liverpool, UK*, 4–6, 2008.
- Houze, J. A., Rasmussen, K. L., Medina, S., Brodzik, S. R., and Romatschke, U.: Anomalous atmospheric events leading to the 2010 floods in Pakistan, *B. Am. Meteorol. Soc.*, 92, 291–298, 2011.
- 20 Larry, W. and Neill, O.: Surface wind modification near mid-latitude ocean fronts: observational and dynamic analysis, PhD thesis, UMI Microform, ProQuest Information and Learning Company, Michigan, USA, 181–183, 2007.
- Lau, W. K. M. and Kim, K.-M.: The 2010 Pakistan flood and Russian heat wave: teleconnection of hydrometeorological extremes, *J. Hydrometeorol.*, 13, 392–403, doi:10.1175/JHM-D-11-016.1, 2012.
- 25 Murphy, P. P., Feely, R. A., Gammon, R. H., Harrison, D. E., Kelly, K. C., and Waterman, L. S.: Assessment of the air–sea exchange of CO<sub>2</sub> in the South-Pacific during austral autumn, *J. Geophys. Res.-Oceans*, 96, 20455–20465, 1991.
- 30 Neill, O., Chelton, L. W. D. B., and Esbensen, S. K.: Observations of SST-induced perturbations of the wind stress field over the Southern Ocean on seasonal timescales, *J. Climate*, 16, 2340–2354, 2003.

## Dynamic variability examination of Mediterranean frontogenesis

B. A. Munir et al.

[Title Page](#)

[Abstract](#)

[Introduction](#)

[Conclusions](#)

[References](#)

[Tables](#)

[Figures](#)

[⏪](#)

[⏩](#)

[◀](#)

[▶](#)

[Back](#)

[Close](#)

[Full Screen / Esc](#)

[Printer-friendly Version](#)

[Interactive Discussion](#)



Nieto, K., Demarcq, H., and McClatchie, S.: Mesoscale frontal structures in the Canary Upwelling System: new front and filament detection algorithms applied to spatial and temporal patterns, *ELSEVIER, Remote Sens. Environ.*, 123, 339–346, doi:10.1016/j.rse.2012.03.028, 2012.

Palmer, C. E.: On high-level cyclones originating in the tropics, *EOS T. Am. Geophys. Un.*, 32, 683–695, 1951.

Pankiewicz, G. S.: Pattern recognition techniques for the identification of cloud and cloud systems, *Meteorol. Appl.*, 2, 257–271, 1995.

Pike, J.: Synoptic scale system, in: *Air Force Weather Agency Doctrine (Volume 1.)*, edited by: Sherman, R., Federation of American Scientist (Space Policy Project), available at: <http://fas.org/spp/military/docops/afwa/atmos-U3.htm>, last access: 5 May 2015), 1999.

Ramage, C. S.: The subtropical cyclone, *J. Geophys. Res.*, 67, 1401–1411, 1962.

Riehl, H.: Venezuelan rain systems and the general circulation of the summer tropics 11: Relations between low and high latitudes, *Mon. Weather Rev.*, 105, 1421–1433, 1977.

Riordan, A. J.: Examination of the mesoscale features of the GALE coastal front of 24–25 January 1986, *Mon. Weather Rev.*, 118, 258–282, 1990.

Simpson, R. H.: Evolution of the Kona Storm, a Subtropical cyclone, *J. Meteorol.*, 9, 24–35, 1952.

Spall, M. A.: Frontogenesis, subduction, and cross-front exchange at upper ocean fronts, *J. Geophys. Res.-Oceans*, 100, 2543–2557, 1995.

Vescio, M. D., Keeter, K. K., Dial, G., Badgett, P., and Riordan, A. J.: A low-top weak-reflectivity severe weather episode along a thermal/moisture boundary in eastern North Carolina, preprints, in: *17th Conference on Severe Local Storms*, St. Louis, MO, 4–8 October 1993, *Amer. Meteor. Soc.*, 629–633, 1993.

Volkert, H.: Components of the Norwegian Cyclone Model: observations and theoretical ideas in Europe prior to 1920, in: *The Life Cycles of Extra-tropical Cyclones AMS*, Boston, 15–28, 1999.

Wang, S. Y., Davis, R. E., Huang, W. R., and Gillies, R. R.: Pakistan's two-stage monsoon and links with the recent climate change, *J. Geophys. Res.*, 116, D16114, doi:10.1029/2011JD015760, 2011.

Webster, P. J., Toma, V. E., and Kim, H.-M.: Were the 2010 Pakistan floods predictable?, *Geophys. Res. Lett.*, 38, L04806, doi:10.1029/2010GL046346, 2011.

## Dynamic variability examination of Mediterranean frontogenesis

B. A. Munir et al.

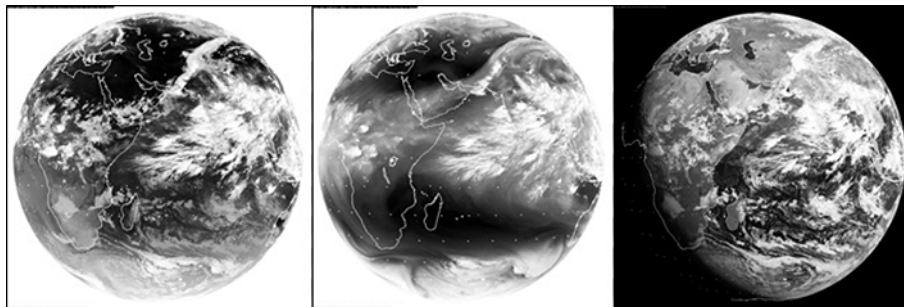


**Figure 1.** Meteosat-7 imagery infra-red (left), water vapor (middle) and visible (right).

[Title Page](#)

[Abstract](#)

[Introduction](#)

[Conclusions](#)

[References](#)

[Tables](#)

[Figures](#)

[⏪](#)

[⏩](#)

[◀](#)

[▶](#)

[Back](#)

[Close](#)

[Full Screen / Esc](#)

[Printer-friendly Version](#)

[Interactive Discussion](#)



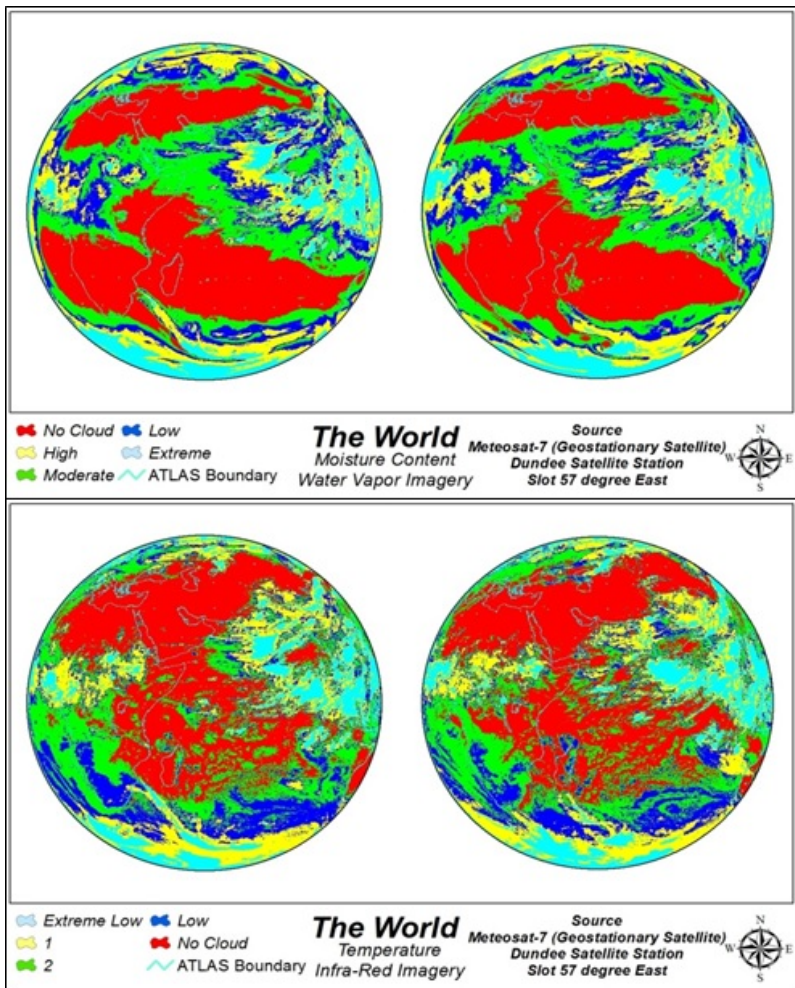


**Figure 2.** Classified images of water vapour and infra-red.

## Dynamic variability examination of Mediterranean frontogenesis

B. A. Munir et al.

[Title Page](#)

[Abstract](#)

[Introduction](#)

[Conclusions](#)

[References](#)

[Tables](#)

[Figures](#)

⏪

⏩

◀

▶

[Back](#)

[Close](#)

[Full Screen / Esc](#)

[Printer-friendly Version](#)

[Interactive Discussion](#)



## Dynamic variability examination of Mediterranean frontogenesis

B. A. Munir et al.

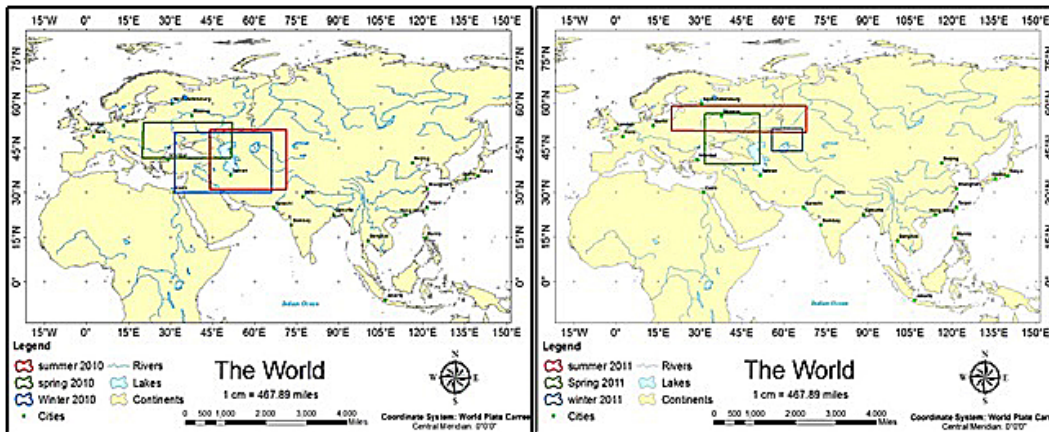


**Figure 3.** Geographical extent of frontogenesis for 2010 and 2011.

[Title Page](#)

[Abstract](#)

[Introduction](#)

[Conclusions](#)

[References](#)

[Tables](#)

[Figures](#)



[Back](#)

[Close](#)

[Full Screen / Esc](#)

[Printer-friendly Version](#)

[Interactive Discussion](#)



**Dynamic variability  
examination of  
Mediterranean  
frontogenesis**

B. A. Munir et al.

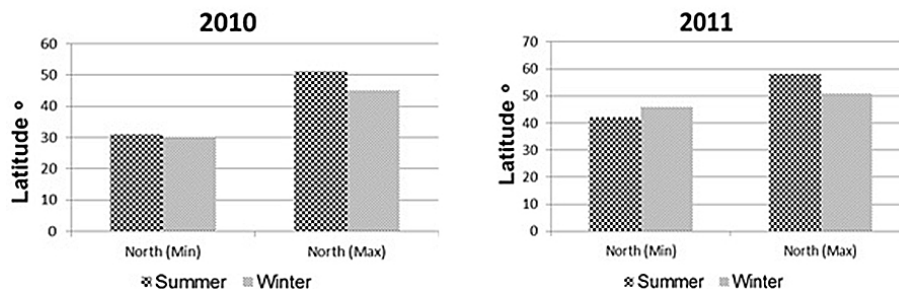


**Figure 4.** Latitudinal limits of frontogenesis for the year 2010 and 2011 in summer and winter.

[Title Page](#)[Abstract](#)[Introduction](#)[Conclusions](#)[References](#)[Tables](#)[Figures](#)[⏪](#)[⏩](#)[◀](#)[▶](#)[Back](#)[Close](#)[Full Screen / Esc](#)[Printer-friendly Version](#)[Interactive Discussion](#)

**Dynamic variability  
examination of  
Mediterranean  
frontogenesis**

B. A. Munir et al.

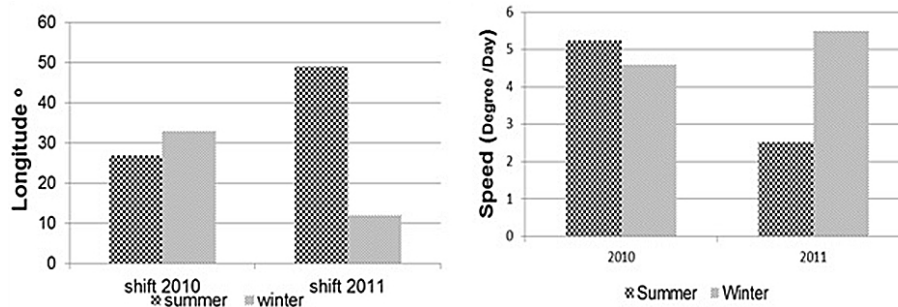


**Figure 5.** Longitudinal shift (left) and speed of front (right) for 2010 and 2011.

[Title Page](#)[Abstract](#)[Introduction](#)[Conclusions](#)[References](#)[Tables](#)[Figures](#)[⏪](#)[⏩](#)[⏴](#)[⏵](#)[Back](#)[Close](#)[Full Screen / Esc](#)[Printer-friendly Version](#)[Interactive Discussion](#)

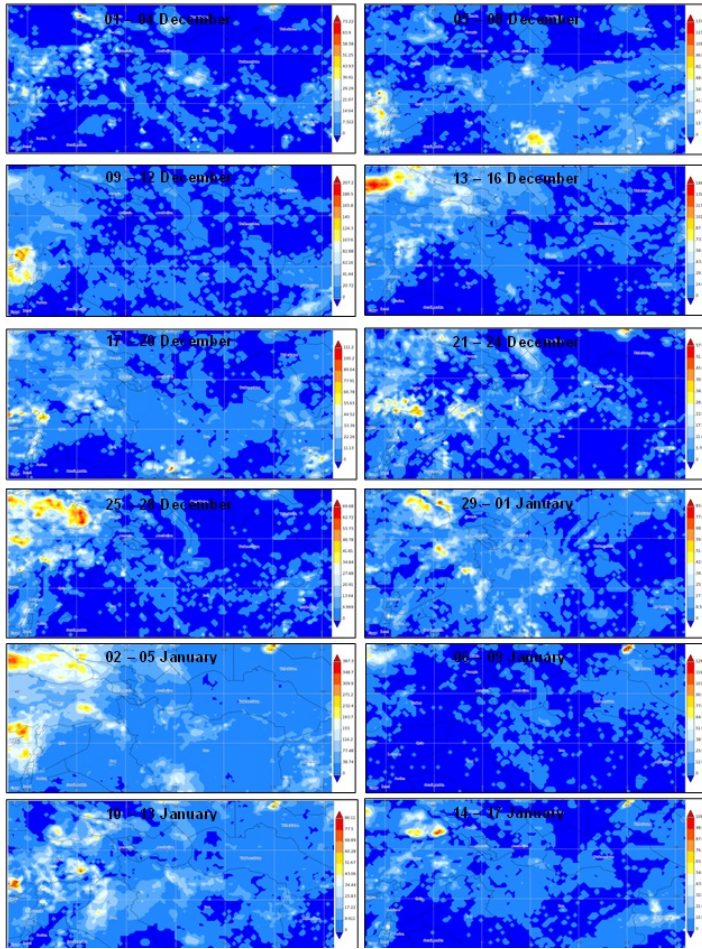


**Figure 6.** Rainfall distribution over geographically delineated extent of frontogenesis in winter 2010.

## Dynamic variability examination of Mediterranean frontogenesis

B. A. Munir et al.

[Title Page](#)

[Abstract](#)

[Introduction](#)

[Conclusions](#)

[References](#)

[Tables](#)

[Figures](#)

[⏪](#)

[⏩](#)

[◀](#)

[▶](#)

[Back](#)

[Close](#)

[Full Screen / Esc](#)

[Printer-friendly Version](#)

[Interactive Discussion](#)



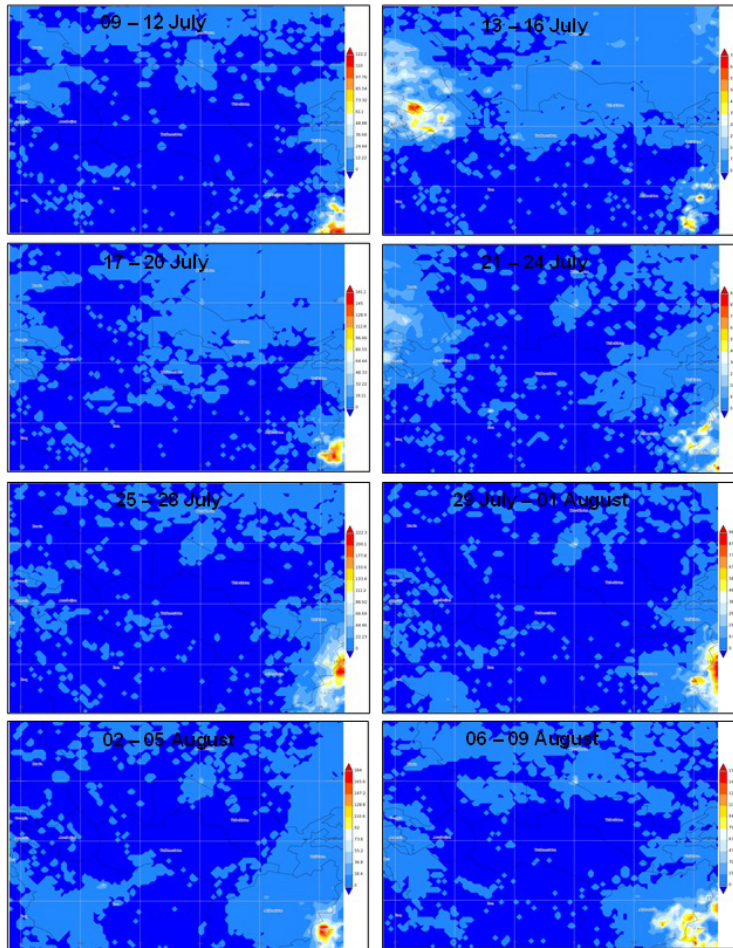


**Figure 7.** Rainfall distribution over geographically delineated extent of frontogenesis in summer 2010.

## Dynamic variability examination of Mediterranean frontogenesis

B. A. Munir et al.

[Title Page](#)

[Abstract](#)

[Introduction](#)

[Conclusions](#)

[References](#)

[Tables](#)

[Figures](#)

[⏪](#)

[⏩](#)

[◀](#)

[▶](#)

[Back](#)

[Close](#)

[Full Screen / Esc](#)

[Printer-friendly Version](#)

[Interactive Discussion](#)



## Dynamic variability examination of Mediterranean frontogenesis

B. A. Munir et al.

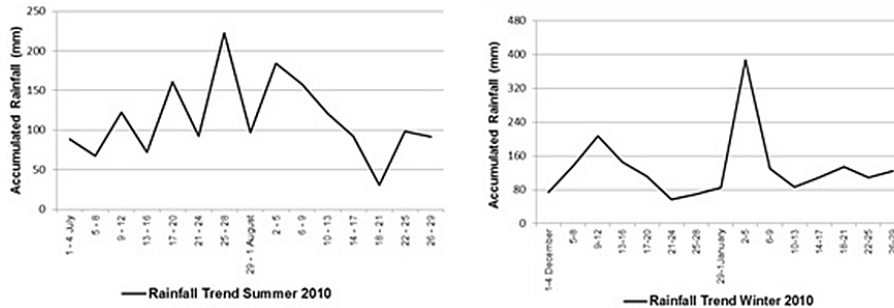


**Figure 8.** Peak four days accumulated rainfall trends for summer and winter 2010.

Title Page	
Abstract	Introduction
Conclusions	References
Tables	Figures
◀	▶
◀	▶
Back	Close
Full Screen / Esc	
Printer-friendly Version	
Interactive Discussion	



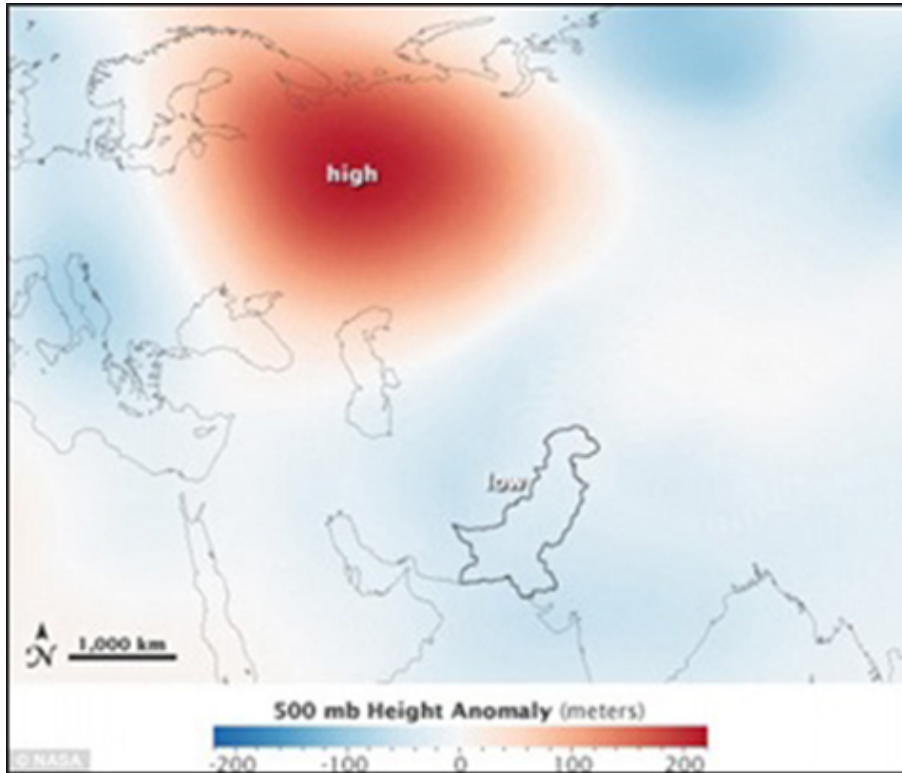


**Figure 9.** High and Low distribution over Russia and Pakistan (source: Allen, 2011).

## Dynamic variability examination of Mediterranean frontogenesis

B. A. Munir et al.

[Title Page](#)

[Abstract](#)

[Introduction](#)

[Conclusions](#)

[References](#)

[Tables](#)

[Figures](#)

[⏪](#)

[⏩](#)

[⏴](#)

[⏵](#)

[Back](#)

[Close](#)

[Full Screen / Esc](#)

[Printer-friendly Version](#)

[Interactive Discussion](#)



## Dynamic variability examination of Mediterranean frontogenesis

B. A. Munir et al.

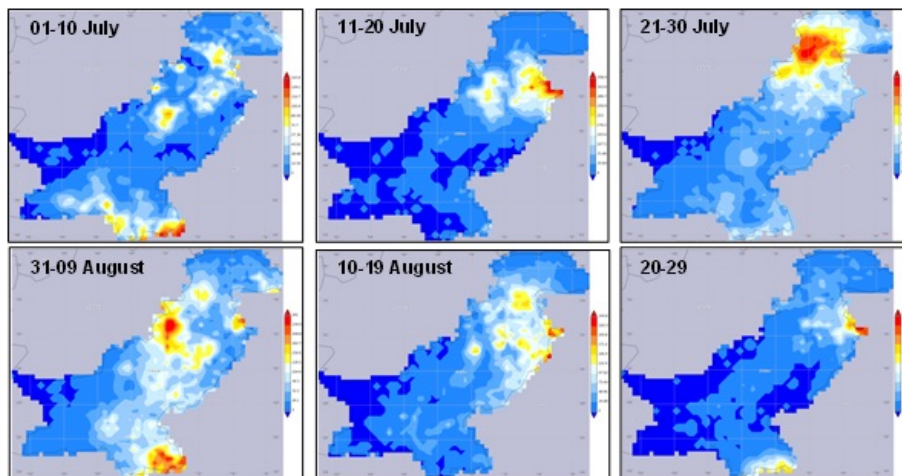


**Figure 10.** Rainfall distribution (mm) over Pakistan during July and August 2010.

[Title Page](#)

[Abstract](#)

[Introduction](#)

[Conclusions](#)

[References](#)

[Tables](#)

[Figures](#)

[⏪](#)

[⏩](#)

[◀](#)

[▶](#)

[Back](#)

[Close](#)

[Full Screen / Esc](#)

[Printer-friendly Version](#)

[Interactive Discussion](#)



## Dynamic variability examination of Mediterranean frontogenesis

B. A. Munir et al.

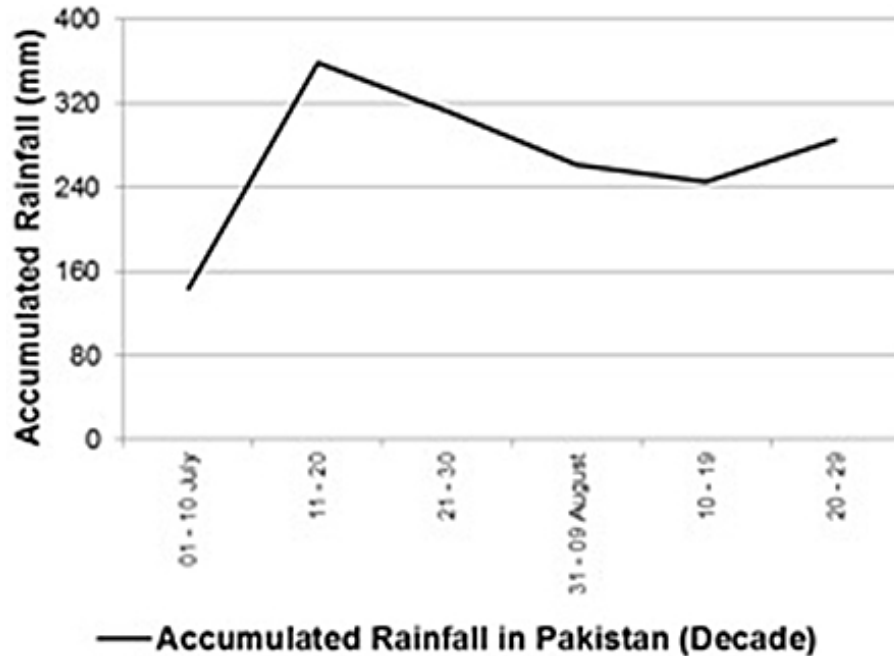


**Figure 11.** Decadal based accumulated peak rainfall for July and August 2010.

[Title Page](#)

[Abstract](#) | [Introduction](#)

[Conclusions](#) | [References](#)

[Tables](#) | [Figures](#)

[◀](#) | [▶](#)

[◀](#) | [▶](#)

[Back](#) | [Close](#)

[Full Screen / Esc](#)

[Printer-friendly Version](#)

[Interactive Discussion](#)

